# A Novel Broadband Multilevel Fast Multipole Algorithm With Incomplete-Leaf Tree Structures for Multiscale Electromagnetic Problems

Manouchehr Takrimi, *Student Member, IEEE*, Özgür Ergül, *Senior Member, IEEE*, and Vakur B. Ertürk, *Member, IEEE*

***Abstract*— An efficient and versatile broadband multilevel fast multipole algorithm (MLFMA), which is capable of handling large multiscale electromagnetic problems with a wide dynamic range of mesh sizes, is presented. By invoking a novel concept of incomplete-leaf tree structures, where only the overcrowded boxes are divided into smaller ones for a given population threshold, versatility of using variable-sized boxes is achieved. Consequently, for geometries containing highly overmeshed local regions, the proposed method is always more efficient than the conventional MLFMA for the same accuracy, while it is always more accurate if the efficiency is comparable. Furthermore, in such a population-based clustering scenario, the error is controllable regardless of the number of levels. Several canonical examples are provided to demonstrate the superior efficiency and accuracy of the proposed algorithm in comparison with the conventional MLFMA.**

***Index Terms*— Broadband solvers, incomplete leaf (IL), low-frequency breakdown, multilevel fast multipole algorithm (MLFMA), multiscale problems.**

## I. Introduction

ALTHOUGH the method of moments (MoM) [1] has been verified to be one of the most versatile and accurate techniques to solve radiation and scattering problems, it has some serious disadvantages regarding memory consumption and CPU time even for today's powerful computers. Hence, fast and accurate solvers have been developed based on iterative solutions of matrix equations along with specialized acceleration techniques for matrix-vector multiplications (MVMs) to empower this method. Some of the well-known methods to accelerate the MoM are the fast multipole method (FMM) [2], multilevel fast multipole algorithm (MLFMA) [3], adaptive integral method [4], QR-based or SVD-based methods [5], and adaptive cross approximation [6]. In many of these and other similar methods, the memory and CPU requirements are reduced from $\mathcal{O}(N^2)$ complexity to $\mathcal{O}(N^\alpha)$ $(1 \leq \alpha \leq 2)$ for single-level implementations and to $\mathcal{O}(N\log^\alpha N)$ for the corresponding multilevel versions, where $N$ denotes the number of unknowns.

The concepts behind FMM and hence MLFMA (as its multilevel version) have provided inspiration for many new and novel computational methods during the last two decades. Regardless of the methodology used in them, the ultimate goal is to increase the efficiency and/or accuracy using a wide variety of analytical or numerical algorithms, matrix manipulation techniques, and diverse parallelization schemes. Considering the accuracy, one can briefly categorize possible error sources commonly encountered in these methods as follows:

1) MoM-related errors due to surface and operator discretizations and integrations over basis and testing functions;
2) FMM-related errors due to truncated summations, computations of special functions over unit sphere, and interpolation/anterpolation operations;
3) other computational errors due to various numerical integrations, compression and decomposition of matrices (if any), and residual errors in iterative solutions.

For the above-mentioned error sources, there are many primitive and elegant remedies leading to a wide range of novel and practical methods. However, when multiscale electromagnetic problems are considered, such as electrically small, layered, and complicated antennas on large platforms that require highly overmeshed local regions, another source of error or a significant inefficiency originates from the fact that almost all of the above-mentioned methods deploy fixed-size boxes at each and every level of the corresponding tree structures. In such multiscale problems, one may use very dense meshes over the entire geometry to possess the fine details, so that accurate results can be obtained using fixed-size boxes. However, such an attempt is a brute-force solution with a huge number of unknowns requiring an excess amount of memory in addition to being extremely inefficient even when a large number of levels are employed.

A better and widely preferred approach is to use nonuniform meshes to discretize multiscale problems. In this approach, one may use large boxes together with the lower number of levels

Manuscript received July 16, 2015; revised February 17, 2016; accepted March 28, 2016. Date of publication April 11, 2016; date of current version May 30, 2016.

M. Takrimi and V. B. Ertürk are with the Department of Electrical and Electronics Engineering, Bilkent University, Ankara 06800, Turkey (e-mail: takrimi@ee.bilkent.edu.tr; vakur@ee.bilkent.edu.tr).

O. Ergül is with the Department of Electrical and Electronics Engineering, Middle East Technical University, Ankara 06800, Turkey (e-mail: ozgur.ergul@eee.metu.edu.tr).

Color versions of one or more of the figures in this paper are available online at http://ieeexplore.ieee.org.

Digital Object Identifier 10.1109/TAP.2016.2552545

to maintain the desired accuracy. Unfortunately, in this case, an $\mathcal{O}(N^2)$ complexity is inevitable in near-field computations due to boxes enclosing locally overmeshed regions. On the other hand, one can use smaller boxes with some deep levels of the MLFMA to avoid the $\mathcal{O}(N^2)$ complexity. However, leaf level boxes at deep levels are too small to hold basis/testing functions. Parts of the basis/testing functions may be located in different boxes and some of these boxes may even be in the far zone of each other based on the one-buffer-box criterion [7] that is frequently used in MLFMA implementations. Hence, critical computational errors contaminate the accuracy. Furthermore, this error becomes more significant as the multiscale factor, which is defined as the ratio of the largest edge length to the smallest one over the entire meshed surface, increases.

In this paper, we propose a novel broadband incomplete-leaf (IL) MLFMA for multiscale electromagnetic problems by invoking a concept of novel IL tree structures, where only overcrowded boxes (OCBs) are divided into the smaller ones. Furthermore, we provide a complete implementation strategy of the proposed IL-MLFMA by introducing some ground rules to redefine near-box (i.e., classifying near-field interactions) and far-box (i.e., classifying far-field interactions) concepts to ensure efficiency and accuracy.

Therefore, for multiscale problems, in addition to using variable mesh sizes, variable box sizes are used so that both $\mathcal{O}(N^2)$ complexity coming from the near-field calculations of OCBs and the computational errors arising from the protrusion of basis/testing functions are eliminated. In comparison with the conventional MLFMA, the efficiency and accuracy of the proposed IL-MLFMA are revealed better as the multiscale factor increases. An approximate method for the diagonalization of Green's function proposed in [8], which is simple and demonstrated to be stable at arbitrary low-frequencies, is implemented to handle the well-known low-frequency problems of the MLFMA. However, other methods that are proposed to treat this problem [9]–[14] can also be used in conjunction with the proposed IL-MLFMA. Furthermore, the novel IL tree structures reduce to traditional ones and the proposed IL-MLFMA reduces to the conventional MLFMA if desired for uniform meshes. Consequently, the proposed IL-MLFMA can also be combined with the available domain decomposition algorithms, such as the equivalence principle algorithm (EPA) [15], which are usually used together with the conventional MLFMA to attack multiscale electromagnetic problems with very large multiscale factors.

Apart from the EPA, some other methods based on the hierarchical MLFMA [16], multiresolution basis functions [17], and accelerated Cartesian expansion [18] have also been used to attack multiscale problems. In various advanced computing [19], chemistry [20], biology [21], and physics [22] applications, especially in $N$-body problems, a modified version of the FMM, namely, the adaptive FMM, has been used. This method employs an adaptive tree strategy, which visually resembles our proposed IL tree structures using variable-sized boxes. However, these problems deal with $N$ discrete entities (particles, molecules, masses, etc.) with static (and mostly analytical) kernels. Hence, they use the original FMM with variable-sized boxes with a single level only. Extension of the adaptive FMM to dynamic problems and construction of its multilevel version (for the desired complexity) have not been attempted to the best of the authors' knowledge. In fact, a direct extension of the adaptive FMM would be less accurate compared with the proposed IL-MLFMA and it would yield problems when parallelization is concerned, as briefly explained in Section III. We note that the concept of using a simple hybrid tree structure for a multiscale problem was proposed in [23] with only two different box sizes at the leaf level.

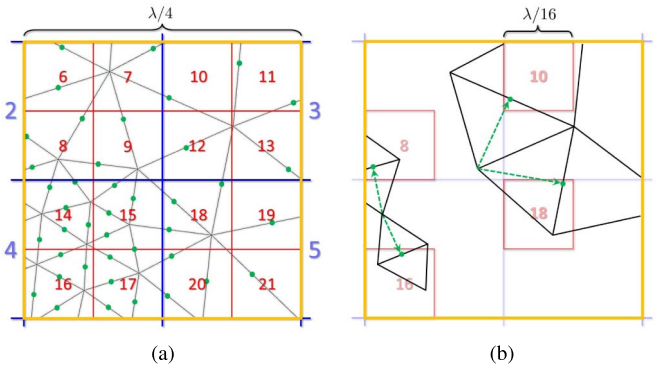


Fig. 1. Simple demonstration of computational errors due to multiscale meshes. (a) Recursive clustering of a multiscale mesh. (b) Some problematic interactions between touching edge-based functions that are interpreted as far field in the given clustering scheme.

The outline of this paper is as follows. Section II presents a brief analysis of the MLFMA tree structure followed by an exposition regarding the new IL tree structure. In Section III, we introduce new concepts of pseudonear interactions and the implementation details of the proposed IL-MLFMA. The simulation results demonstrating the numerical stability, accuracy, and efficiency are given in Section IV based on some canonical problems, followed by our concluding remarks in Section V.

## II. New Tree Structure for Multiscale Meshes

### A. Multiscale Mesh as a Source of Error

To have a clear vision about the imposed errors and the necessity of introducing the new incomplete-leaf concept to overcome them, we consider a flat 2-D mesh with a multiscale factor of 4 in Fig. 1(a). The size of the largest box shown in Fig. 1 is assumed to be $\lambda/4$. Hence, after two consecutive clusterings (i.e., recursively bisecting the boxes in both directions), one reaches to the minimum box size of $\lambda/16$. To demonstrate the borders of some typical boxes in three consecutive MLFMA levels, different colors are used in Fig. 1, where the largest box casts as the top level, four boxes numbered from 2 to 5 as the next lower level, and finally, 16 small boxes numbered from 6 to 21 as the second lower level. Midpoints of all edges are labeled with small circles to track edge-based functions, such as the Rao–Wilton–Glisson (RWG) [24] functions that are used in this work. Based on the three levels and the boxes involved, one can observe two important issues that are interfering with each other.

*1) Considering Box Sizes:*

1) The largest box with a size of $\lambda/4$ contains 40 edges (RWGs). It costs $40^2 = 1600$ near-field interactions by itself and some others with possible nearby boxes.

2) The lower level boxes contain 5 to 19 RWGs. They involve 25 to 361 near-field interactions by themselves and some others with nearby boxes. However, those boxes involve large errors in far-field interactions either due to their small size ($\lambda/8$) or due to those triangles sticking out of the boxes.
3) The lowest level boxes contain one to six RWGs. They involve 1 to 36 near-field interactions by themselves and some others with nearby boxes. Considerable errors regarding far-field interactions occur, mainly due to very small box sizes ($\lambda/16$) and severe protrusions.

Fortunately, deploying broadband solvers [8], [10], [13], [18] can effectively eliminate or at least alleviate box-size-related inaccuracies to some limited extent. This limit is governed by the size of the RWG functions in such a way that after some critical point, one may not have a complete RWG function embedded inside the box of interest. Hence, this limit has a close relation with the multiscale factor and distributions of box populations in each and every level.

*2) Considering Box Populations:*

1) The largest box contains almost 40 RWG functions, but only 17 (42%) of them are completely inside the box.
2) The lower level boxes contain 5–19 RWGs, but only the fourth box contains six (30%) complete functions.
3) The lowest level boxes contain 1–6 RWGs, and none of them contains a complete RWG function.

Thus, by increasing the number of levels over multiscale meshes possessing high multiscale factor, a new error source is introduced regarding the far-field computations. To have an intuition about this effect, consider two boxes, i.e., 18 and 10, that are independently depicted in Fig. 1(b). These two boxes are supposed to be far-field boxes based on the one-buffer-box criterion. Hence, we attempt to use the addition theorem to test the radiated field of an RWG function located inside the 18th box over any RWG function located inside the 10th box. However, both RWG functions have a common node inside the 9th box and even a common edge partially inside the 12th box (the buffer box), which means that they are in fact practically near to each other.

At this stage, we note that if we consider only the edge centers as the source and test points, they completely satisfy the necessary condition for the far-field assumption and thus the addition theorem. However, considering these midpoints as representatives of their corresponding basis and testing functions, this assumption is not valid anymore and their interactions are prone to a considerable error. The same argument holds for the other RWG functions that are protruded out of their corresponding boxes. Increasing the box size effectively diminishes the error, but on the other side, it dramatically increases the computation time due to the increased number of RWGs inside the boxes leading to $\mathcal{O}(N^2)$ complexity in self- and near-field interactions of boxes. Obviously, for real-life large multiscale problems with millions of unknowns, we have no other choice than increasing the number of levels to run away from quadratically increasing the number of near-field interactions. It should be mentioned that this problem becomes worse for 3-D structures.

### *B. Variable Boxes for Multiscale Meshes*

The aforementioned deficiencies arising from large RWG functions inside relatively small boxes can effectively be eliminated by totally modifying the whole clustering strategy: there is no need to divide all the boxes across a given level to create the next level, and therefore, some boxes with a lower RWG population may stay at an upper level, while those with a higher population can be further divided into smaller boxes. While such a clustering strategy seems trivial, its implementation needs a detailed investigation of box–box interactions and their careful organizations for an efficient and accurate solver.

In this paper, we present an implementation, where the boxes with RWG populations exceeding some predetermined threshold (that may be a function of the corresponding level) are split into smaller boxes. This is achieved by letting the program start from an arbitrary level, which is mainly the second level (i.e., the MoM level), and continue the clustering process as far as it takes such that none of the leaf boxes are overpopulated. Note that because the boxes are variable sized, large boxes usually contain large RWG functions, thereby minimizing possible protrusions of them. On the other hand, the novel IL tree structure can be reduced to a traditional one by simply assigning unity population threshold for all higher levels except the leaf level. Then the program starts from the second level and continues the division process equally everywhere up to a maximum allowed level (though some of the last level boxes may be overcrowded), and hence, the conventional MLFMA is recovered.

## III. Implementation

The following concepts and issues must be considered during the implementation of the proposed IL-MLFMA, where MATLAB is used.

### *A. Box Population*

To determine how deep the program has to continue the clustering process, we have to recursively slice the object in three dimensions and record the population statistics across all the levels for two important reasons: 1) to decide whether a box is an overcrowded one or not and 2) to have an educated guess about the proper value of the population threshold specific for that level.

### *B. Incomplete-Leaf Tree and Near- and Pseudonear Box Concepts*

Fig. 2(a) illustrates a six-level nonuniform clustering for an object that might be electrically large and possesses very fine local features. Its 2-D cross sectional view is shown in Fig. 2(b) to provide the readers an intuition about the density of the given mesh all over the surface and the relative sizes of the RWG functions at different levels. Obviously, large boxes on top (i.e., first couple of) levels contain relatively large RWG functions and small boxes at deep levels may contain extremely small RWG functions. To handle such a nonuniform clustering with the MLFMA, we propose the novel IL

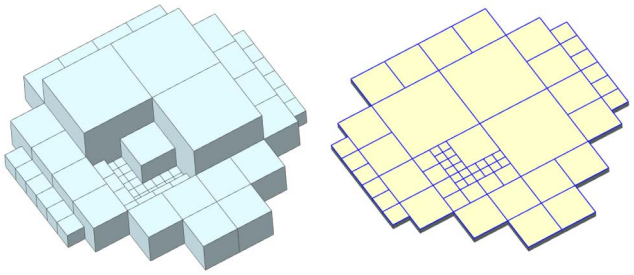

(a) (b)

Fig. 2. (a) 3-D structure of a typical flat object after six levels of nonuniform clustering. (b) Proper cross section as a representative of the corresponding 3-D structure shown in (a).

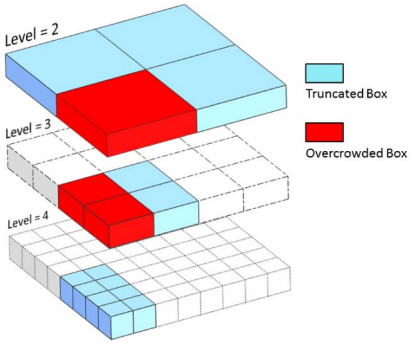


Fig. 3. Typical IL tree structure for a thin object (as a 2-D example, heights are not in scale). TBs and OCBs are shown in light gray (cyan) and dark gray (red), respectively. The white boxes are considered as pruned boxes.

tree structure. In such a tree structure, for a predetermined threshold, which may be fixed or a function of level, two different types of boxes are defined. The first one is an OCB that contains more (or equal) number of RWG functions than the given threshold. An OCB cannot be located at the last level. The second one is a truncated box (TB) that has a less number of RWG functions than the threshold. A TB may exist at any level and no other boxes branches from a TB. Note that TBs are actually new leaves but with distributed positions across different levels. In such a tree, some or many of the branches are incomplete, leading us to a novel IL tree structure.

Fig. 3 illustrates a typical four-level IL tree structure for a thin object (without taking into account the correct height of the boxes), where OCBs and TBs can be seen clearly. Since an IL tree structure is different from a traditional one used by the conventional MLFMA, near-box and far-box concepts are required to be redefined. In addition, some ground rules must be constructed to determine near and far boxes from the accuracy and efficiency point of views. Hence, possible two different 2-D scenarios to determine the near and far boxes in an IL tree structure are illustrated in Fig. 4, where the small shaded box in the middle is the testing box and the surrounding dark gray (red) and light gray (green) boxes denote near and far basis boxes, respectively. The borders for the third to fifth levels are shown in the legend.

The scenario shown in Fig. 4(a) is very similar to an adaptive tree, which is employed in an adaptive FMM (assuming that an adaptive FMM is extended to a dynamic

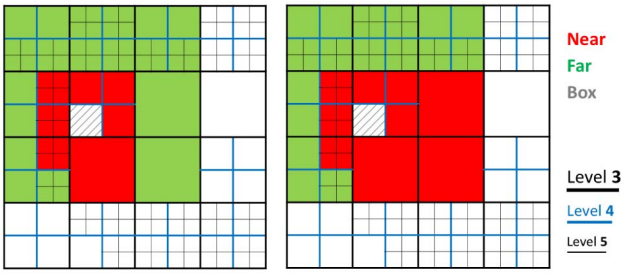


(a) (b)

Fig. 4. Two different scenarios to define near and far boxes, shown by dark gray (red) and light gray (green) boxes, respectively. (a) Near boxes based on touching boxes. (b) Near boxes based on either touching boxes or larger near boxes at higher levels. Far boxes are defined as the rest of the boxes inside a proper cuboid of size $6 \times 6 \times 6$ at the corresponding level.

electromagnetic problem and its multilevel version is constructed). Based on this scenario, only touching boxes with equal or larger sizes are labeled as near boxes. However, when the second scenario shown in Fig. 4(b) is considered, unclustered near boxes of all the upper level parents, if exist, are added to those boxes found in the first scenario. For example, additional two level-3 large (i.e., unclustered) boxes should also be considered as near boxes for the parent of the shaded box. Then, in both scenarios, far boxes are determined by the rest of the boxes that reside inside a proper $6\times6\times6$ cuboid of the same size (of the shaded box). A detailed comparison between these two scenarios reveals that although the second scenario is more complicated to implement, it is more superior than the first one due to the following two reasons.

1) For the scenario shown in Fig. 4(a), consecutive interpolation and anterpolation operations are needed for both aggregation and disaggregation processes within MVM routines. The reason is that there are a few larger, some equal, and some other smaller far boxes for which the far-field interactions should be calculated using the FMM. Consequently, for these boxes at the very same level (i.e., level 4, referring to Fig. 4), one needs an anterpolation, a direct calculation, and an interpolation, respectively, each followed by a proper translation to carry out the far-field interactions correctly. These extra computations based on the FMM (and not MoM) bring in undesired additional errors. On the other hand, using different-sized boxes and the one-buffer-box scheme pushes the limits of the addition theorem if the buffer box is smaller than any of them. It should be emphasized that an interpolation/anterpolation operation brings additional challenges in parallelization.
2) For the scenario shown in Fig. 4(b), larger boxes are treated via MoM computations leading to higher accuracy without any of the above-mentioned issues.

Two important issues should also be noted at this point.

1) Although the scenario shown in Fig. 4(b) has more near-field interactions than the scenario in Fig. 4(a) (so that it improves the accuracy but leads to a higher computational cost), the total number of near-field

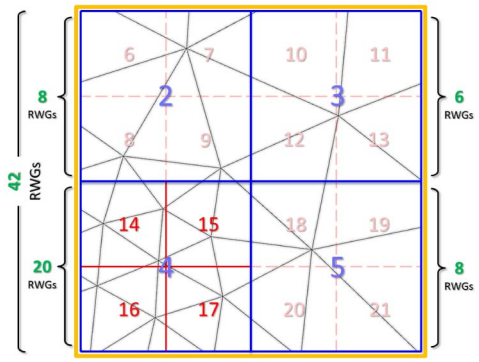


Fig. 5. Applying IL tree clustering on the multiscale mesh of Fig. 1. The numbers given next to the curly braces show RWG populations of the corresponding boxes. Only the largest box and the fourth box are divided into four smaller boxes. All pruned boxes are designated by light gray numbers.

interactions are controllable [and in fact $\mathcal{O}(N)$] as there is no practical limit regarding the needed levels. This will be addressed in the numerical results (Section IV), where we discuss the complexity of the proposed algorithm.

2) The total number of interacting boxes is always less than the conventional MLFMA due to the pruned boxes that were supposed to branch from TBs across the levels.

Finally, in many multiscale problems that have to be meshed nonuniformly with large multiscale factors, one can see some special boxes that belong to upper level parents and are located farther than some of the far boxes at the same level, based on the scenario shown in Fig. 4(b). These boxes, hereafter to be called pseudonear boxes, are defined as nontouching TBs located at any upper level that have the following three properties.

1) They are larger than the box of interest (the gray box).
2) They can be classified as touching near boxes for the parent or any of the grandparents of the box of interest.
3) They cannot be smaller than the size of the parent or the grandparent to be compared in step 2).

Such a definition justifies its appellation and helps us to distinguish these boxes from the real near boxes that touch each other. Note that touching boxes may be smaller, equal, or larger than the testing box, but pseudonear boxes are always larger, because they usually contain larger basis functions. The importance of this pseudonear concept can be displayed best by once again considering Fig. 1(a). By clustering the same mesh using the proposed IL tree structure for a given population threshold, Fig. 5 is obtained, where the numbers near the curly braces show the RWG populations. Only the largest box and the 4th box are divided into four smaller boxes, namely, 2–5 and 14–17, respectively, since their populations are larger than or equal to the given threshold. Considering the small box labeled 17 and applying the aforementioned ground rules used to determine the near and far boxes, apart from the trivial near boxes 14, 15, 16, and 5, there are two larger pseudonear boxes labeled 2 and 3. When the large RWG functions extended into the 2nd and 3rd boxes are considered, most of the RWG functions inside the 17th box are connected to them justifying our rule that all RWG functions inside a pseudonear box of a testing box should indeed have near-field interactions with the RWG functions inside the testing box regardless of the distance between the testing box and the pseudonear box.

It should be emphasized that such a treatment, i.e., dealing with some of the far boxes as if they are near boxes and, hence, computing MoM-based interactions instead of FMM-based interactions do not imperil the philosophy behind deploying the one-buffer-box scheme in the proposed structure. As a corollary fact, we can strongly claim that the robustness and reliability of the proposed method are inherited from those of the conventional MLFMA.

**Algorithm 1** Construction of IL Near List

```
   Input: given level, traditional near list
   Output: IL.NearList
1  TB.List := List of TBs within the given level
2  foreach TestingBox ∈ TB.List do
3      Trad.NearList := traditional near list for TestingBox
4      foreach BasisBox ∈ Trad.NearList do
5          if BasisBox ∈ TBs then
6              put −BasisBox into IL.NearList of TestingBox
7          else if BasisBox ∈ OCBs then
8              put +BasisBox into IL.NearList of TestingBox
9              Trunc.SubBoxes := ContentBoxes (BasisBox)
10             foreach SubBox ∈ Trunc.SubBoxes do
11                 put −TestingBox into IL.NearList of SubBox
12             end
```

### C. Construction of a List of Near and Pseudonear Boxes

Construction of a list of near-field interactions containing all of the near and pseudonear boxes of a given testing box is an important aspect of the proposed method and only the TBs must be considered. OCBs are not considered because if an OCB is near or pseudonear to any given TB, then all the smaller sub-boxes inside that OCB are also considered as the pseudonear boxes with respect to the given TB. From the programming point of view, this means that the very same TB should be added to the so-called near list of all the smaller sub-boxes, which reside inside the OCB, and this operation must be repeated across all the levels from top to bottom.

The pseudocode shown in Algorithm 1 is used to construct the near list for each level. The script used in the given algorithm, namely, ContentBoxes, is responsible for traversing the traditional tree structure to find all the TBs (leaf boxes) inside a given OCB. Note that a positive box number is used for an OCB and a negative box number is used for a TB. Hence, the $-$ sign used in lines 6 and 11 and the $+$ sign used in the line 8 are important, since they facilitate discriminating OCBs from TBs within the list. It is worth mentioning that the resulting near list is actually a matrix with a high degree of sparsity, which heavily depends on the population statistics and the geometrical details of the object.

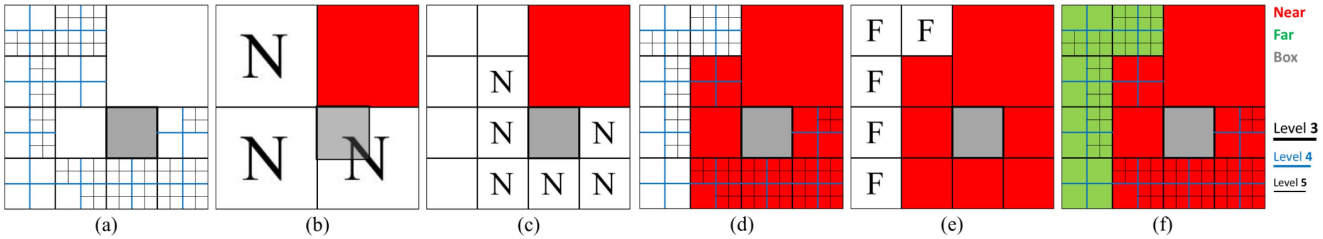


Fig. 6. Step-by-step pictorial approach to determine both near and far boxes for a given testing box inside a typical IL tree structure. (a) Box of interest in gray. (b) First near box. (c) Group of next level near boxes. (d) All near boxes together regardless of size or level. (e) Far boxes at the same level. (f) All far (and near) boxes regardless of size or level. Higher level boundaries always coincide with the lower level boundaries and consequently cover their designated color or thickness in (a)–(f). Note that near and far boxes are shown in dark gray (red) and light gray (green), respectively.

**Algorithm 2** Construction of IL Far List

**Input**: given level, traditional far list
**Output**: IL.FarList

```
1 Joint.List := List of TBs ∪ OCBs within the given level
2 foreach TestingBox ∈ Joint.List do
3     Trad.FarList := traditional far list for TestingBox
4     foreach BasisBox ∈ Trad.FarList do
5         if BasisBox ∈ TBs then
6             put −BasisBox into IL.FarList of TestingBox
7         else if BasisBox ∈ OCBs then
8             put +BasisBox into IL.FarList of TestingBox
```

### *D. Construction of a List of Far Boxes*

Another important aspect of the proposed method is to construct a list of far-field interactions of a given testing box, where the same rules used in the conventional MLFMA to determine the boundaries of the far boxes are deployed. Briefly, we move at least two and at most three boxes in all three directions and stop at the boundaries of either the object itself or one of the parent boxes, whichever comes first. Using this approach, there will be no chance for any larger box in the vicinity to act as a far box, in order to carry out the far-field interactions. By invoking the same policy regarding negative and positive box numbers, we can reuse the proposed near list algorithm by eliminating the lines between 9 and 12 and considering two important facts.

1) Unlike the near list, the OCBs have to be processed accordingly, because one needs to aggregate the radiation of the smaller sub-boxes inside those OCBs.
2) One has to start from the third level, where the far field interactions make sense.

Algorithm 2 shows the pseudocode to construct the far list.

### *E. Pictorial Examples*

Some interesting 2-D geometries are considered to illustrate the near, pseudonear, and far boxes of a given testing box. The near list algorithm works based on a hierarchy implied by the line 9 of Algorithm 1, which means one has to first process the larger boxes at the upper levels, and then process the next level smaller boxes and so on. Note that this is not necessary for the far list algorithm. To start with, we consider a simple case shown in Fig. 6(a), where the given testing box is in gray.

1) The only TB in level 2 is shown in dark gray (red) in Fig. 6(b). All three near boxes of this TB in this level, which are OCBs, are labeled with the letter N. However, the gray box (i.e., the testing box) is the sub-box of only one of them. Hence, the remaining OCBs are not our interest and the TB is the first member of our near list.
2) Considering level 3, Fig. 6(a) also shows that there are only two TBs in this level, which are near to each other. One of them is the testing box and the other one is the second member of the near list. However, referring to Fig. 6(c), boxes labeled with N are also the members of the near list at this level. Fig. 6(d) illustrates all the near boxes including level-wise details.
3) For the far boxes, we must move at least two and at most three boxes from the given test box. However, we also need to stop at the object boundaries. Fig. 6(e) and (f) show all the far boxes labeled with the letter F and the final structure including all details, respectively.

A more complicated and peculiar structure, as shown in Fig. 7(a), is considered next, where the same strategy is followed.

1) Starting from level 2, only the TB is shown in dark gray (red) in Fig. 7(b). As before, all three near boxes to this TB of this level are labeled with N, where the test box is inside one of them. Similar to the first example, the other boxes labeled with N are OCBs and are not considered at this level. Hence, the large dark gray box is the first member for the near list as a pseudonear box.
2) Referring back to Fig. 7(a), we can see three level-3 TBs labeled 1–3 in Fig. 7(c). Neither box 1 nor box 2, with opposite cross-hatched shaded regions, may have near-field interactions with the small gray box. Proceeding to Fig. 7(d), the box labeled 3 is the only level-3 box having near-field interaction with the given test box, and thus it will be the member of the near list again as a pseudonear box.
3) There is only one level-4 TB near to the test box, as shown in Fig. 7(e). In a fashion similar to the previous cases, this TB is also a member of the near list as a near box. Considering the level of the test box, the touching seven boxes are the members of the near list. Fig. 7(f) shows all near and pseudonear boxes.

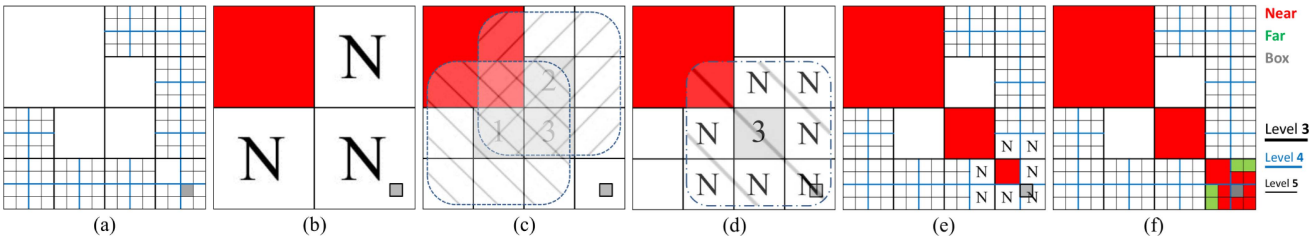


Fig. 7. Another pictorial example to determine the near, pseudonear, and far boxes inside a symmetric IL tree structure. (a) Box of interest in gray. (b) First pseudonear box. (c) None of the two boxes labeled 1 and 2 can cover the gray box. (d) Only the third box is pseudonear to the gray box. (e) Same procedure but with the next level smaller boxes. (f) All the near, pseudonear, and far boxes in one shot.

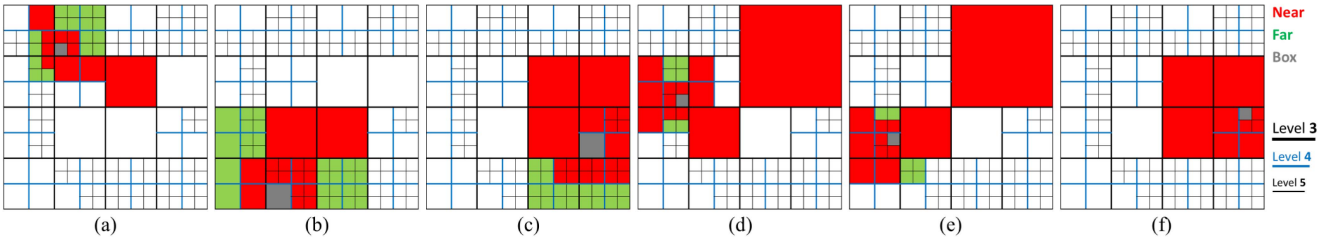


Fig. 8. For a nonuniform clustering, six examples illustrating the near, pseudonear, and far basis boxes regarding a given testing box. A different testing box is considered in (a)–(f). (f) There is no far box due to some large and very large nearby-basis boxes.

4) To find far boxes, if we move down or right, object boundary comes first; however, if we move up or left, the level-4 box boundaries come first. Hence, after excluding all near boxes, we end up with the indicated far boxes, as also illustrated in Fig. 7(f).

More complicated examples are shown in Fig. 8 without step-by-step details about how we apply the ground rules and the related strategies. Note that in Fig. 8(f), there is no far box mainly because of large and very large nearby-basis boxes.

### *F. Near-Field Interactions*

To compute the near-field interactions based on the aforementioned near list (which is actually a matrix with a high degree of sparsity as mentioned before), one has to consider two important facts.

1) The testing/basis functions exist only inside TBs.
2) Within the near list of a given testing box, there may be a combination of TBs together with some other OCBs. Each one of the OCBs may also contain some other OCBs in a recursive manner and this may extend to the very last level.

Using pseudocodes, Algorithm 3 briefly describes the steps to perform this task.

**Algorithm 3** Near-Field Sparse Matrix

```
Input: IL.NearList
Output: Near-Field Sparse Matrix
foreach TestingBox ∈ All of the TBs do
    Mixed.List := List of near and pseudo-near boxes
    regarding TestingBox using IL.NearList
    Final.NearList := Negative elements of Mixed.List
    Overcrowded.List := Positive elements of Mixed.List
    foreach TmpBox ∈ Overcrowded.List do
        Content.List := List of all TBs inside TmpBox
        Final.NearList := Final.NearList ∪ Content.List
    TestingBox△s := List of △s inside TestingBox
    foreach BasisBox ∈ Final.NearList do
        BasisBox△s := List of △s inside BasisBox
        foreach testing△ ∈ TestingBox△s do
            Compute integration points over testing△
            foreach basis△ ∈ BasisBox△s do
                Compute integration points over basis△
                forall the valid testing functions do
                    forall the valid basis functions do
                        Invoke singularity extraction routines
                        to compute formulation dependent
                        integrals (e.g. MFIE)
                        Update Near-Field Sparse Matrix
```

### *G. Far-Field Interactions*

The calculation of far-field interactions is one of the most challenging parts of the proposed IL-MLFMA. Apart from the implementation difficulties due to variable box sizes inside a level and/or across multiple levels, special care is required at low frequencies, where the box sizes become electrically small (i.e., the low frequency problem). Hence, an approximate method for the diagonalization of Green's function, developed in [8], which is simple and demonstrated to be stable at arbitrary low frequencies, is used in conjunction with the proposed IL-MLFMA when the box size is smaller than $\lambda/4$ to treat the low-frequency problem. Consequently, a smooth transition from the low-frequency regime to the high-frequency regime is obtained with an overall complexity of $\mathcal{O}(N \log^{\alpha} N)$, where $(1 \leq \alpha \leq 2)$ ($\alpha = 2$ for the low-frequency regime).

TABLE I

TIMING AND ERROR OF THE IL-MLFMA APPLIED TO A PEC SPHERE OF $R = 5$ cm AT $f = 3.0$ GHz CONSISTING OF 11 343 RWG FUNCTIONS WITH A MULTISCALE FACTOR OF 110, AS A FUNCTION OF MBP

| MBP | 2700 | 2500 | 2350 | 2200 | 1000 | 500 | 300 | 200 | **100** | **90** | **60** | **50** | 20 |
|---|---|---|---|---|---|---|---|---|---|---|---|---|---|
| Maximum Level | 2 | 3 | 4 | 5 | 6 | 7 | 7 | 8 | 8 | 8 | 9 | 9 | 10 |
| Tree (sec) | 1.1 | 1.81 | 2.8 | 4 | 5.4 | 4.3 | 6.8 | 8.4 | 9 | 8.4 | 10.4 | 10.5 | 15.5 |
| Near-field Time (sec) | 2961 | 2977 | 2896 | 2738 | 1972 | 1880 | 968 | 672 | 405 | 375 | 312 | 275 | 82 |
| Solution Time (sec) | 344 | 354 | 427 | 393 | 427 | 495 | 498 | 567 | 672 | 689 | 756 | 812 | 1153 |
| Iteration | 64 | 64 | 64 | 64 | 64 | 64 | 64 | 64 | 64 | 64 | 64 | 64 | 65 |
| Total Run-Time (sec) | 3316 | 3344 | 3336 | 3146 | 2415 | 2391 | 1484 | 1259 | **1099** | **1084** | **1091** | **1110** | 1263 |
| Rel. RMS Error (%) | 2.757 | 2.755 | 2.750 | 2.731 | 2.728 | 2.731 | 2.699 | 2.617 | **2.617** | **2.617** | **2.614** | **2.613** | 2.543 |

**Algorithm 4** Aggregation in the Low-Frequency Regime

**Input**: TBs, OCBs
**Output**: Aggregation Sparse Matrix
**foreach** level ∈ low frequency levels **do**
  Joint.List := List of TBs ∪ OCBs within the level
  Compute $N_\theta$, $N_\phi$ as the numbers of needed samples
  $\theta_i := \theta$ locations over unit sphere
  $\phi_j := \phi$ locations over unit sphere
  **foreach** BasisBox ∈ Joint.List **do**
    **foreach** basis function inside BasisBox **do**
      **foreach** $(\theta_i, \phi_j), i = 1 : N_\theta;\ j = 1 : N_\phi$ **do**
        Compute radiation functions (regarding needed formulation)
        Update Aggregation Sparse Matrix

Important features of the aggregation, translation, and disaggregation operations regarding the far-field interactions are as follows.

*1) Aggregation:* Aggregation for the low-frequency regime and aggregation for the high-frequency regime slightly differ from each other.

*a) Aggregation in the low-frequency regime:* During the construction of the IL tree structure, the box size in each level must be compared with the box sizes in different upper and lower limits to assign a proper scale factor. These optimized scale factors are based on experimentally tabulated values (Table I) [8]. A scale being less than one implies a level that requires low-frequency treatments. In the low-frequency regime, there is no need to perform any interpolation between the successive layers [8]. Hence, Algorithm 4 is applied across the designated levels, where only the TBs and the OCBs are processed.

*b) Aggregation in the high-frequency regime:* The main difference with respect to the aggregation in the low-frequency regime comes from the fact that OCBs need to be processed using interpolation operations. Hence, Algorithm 4 can be used twice: one for the TBs without interpolation and another one for the OCBs with proper interpolation from the lower levels.

*2) Translation:* This operation is the same as that of the conventional MLFMA, where both OCBs and TBs are processed at each and every level. Besides, in the low-frequency regime, [8, eq. (8)] reveals that a scale factor (i.e., $s^t$, where $t$ is the summation index) less than one is used inside the summation and $s$ becomes one as we move to the high-frequency regime.

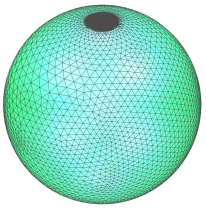

Fig. 9. PEC sphere of radius $R = 5$ cm possessing a dense discretization around the north pole with a multiscale factor of 110.

*3) Disaggregation:* Similar to the aggregation part, two slightly different disaggregation operations are required for the low-frequency and high-frequency regimes.

*a) Disaggregation in the low-frequency regime:* Because the levels are independent of each other, there is no need for anterpolation operations between the successive levels. Consequently, both TBs and OCBs are processed the same way. An algorithm similar to Algorithm 4 can be used.

*b) Disaggregation in the high-frequency regime:* It is similar to its counterpart aggregation process, except the need for anterpolation operation. Hence, for OCBs, the translated values collected from the far-field boxes (listed in the far list) are first anterpolated, and then the updated values are tested either in the lower levels or, maybe, at the last level of the tree structure designated for high-frequency regime. On the other hand, for TBs, the anterpolation operation is not required and the procedure used in the conventional MLFMA can be applied.

## IV. NUMERICAL RESULTS AND DISCUSSION

A perfect electric conductor (PEC) sphere of radius $R = 5$ cm ($\lambda/2$) at $f = 3.0$ GHz with a nonuniform mesh, as illustrated in Fig. 9, is used to investigate the accuracy and the run time of the IL-MLFMA. The edge size for the triangles varies from 0.135 mm ($\lambda/740$) at the north pole up to 15 mm ($\lambda/7$) at the south pole resulting a nonuniform mesh that has a multiscale factor of approximately 110 and consisting of 11343 RWG functions. In all simulations, the magnetic field integral equation (MFIE) formulation is used due to its stability at low frequencies. Besides, in all simulations, the

second-order Gaussian quadrature is used in the integrations over the surfaces of triangles to capture rapid field variations in near-field computations. With regard to the far-field computations, since the order of quadrature does not affect the accuracy significantly, the first-order Gaussian quadrature is used to carry out the far-field interactions from the efficiency point of view. Furthermore, the solutions are obtained without any preconditioning using the generalized minimal residual iterative solver with an error tolerance of $10^{-3}$ and a restart value of 100, while the maximum number of iterations is fixed at 1000.

The results obtained from the IL-MLFMA are compared with those of the Mie-series approach, which is an analytic method for scattering from PEC sphere problems. To assess the accuracy of the IL-MLFMA, the relative root-mean-square (RMS) error is used, given by

$$\text{Relative RMS Error} = \sqrt{\frac{\sum_{i=1}^{N} \left| \boldsymbol{E}_{\theta_i}^{\text{Sim}} - \boldsymbol{E}_{\theta_i}^{\text{Mie}} \right|^2}{\sum_{i=1}^{N} \left| \boldsymbol{E}_{\theta_i}^{\text{Mie}} \right|^2}} \quad (1)$$

where $\boldsymbol{E}_{\theta_i}^{\text{Sim}}$ and $\boldsymbol{E}_{\theta_i}^{\text{Mie}}$ are the dominant $\theta$ component of the far-zone electric field obtained from the IL-MLFMA and the Mie-series solution, respectively.

Table I shows the run times and the relative RMS errors of the IL-MLFMA for the geometry depicted in Fig. 9 as a function of maximum box population (MBP, i.e., population threshold). Note that MBP is the key parameter, which determines the number of levels in the IL-MLFMA.

Regarding the run time, we may arrive at the following conclusions.

1) The construction of the IL tree, though it is more complicated, takes at most 1% of the total run time.
2) The processing time required to fill the near-field matrix decreases as the value of MBP decreases. On the other hand, due to the growing tree structure, the solution time increases. Therefore, there is an optimal value of MBP for the best efficiency in terms of the total time. This optimal value is between 50 and 250 for different problems.
3) Based on a wide range of simulations, it has been observed that the IL-MLFMA always converges regardless of the value of MBP.

On the other hand, regarding the accuracy, we may arrive at the following conclusions based on Table I.

1) When using optimal MBPs in terms of efficiency, we observe that the majority of the triangles do no stick out of the boxes. Hence, the accuracy is almost independent of the number of levels. This is important because it provides us the opportunity to only optimize the total run time rather than accuracy as a function of MBP.
2) The relative RMS error observed in the IL-MLFMA results is comparable with that of MoM.

Next, the same PEC sphere, depicted in Fig. 9, is used to compare the efficiency and accuracy of the IL-MLFMA with (a) the conventional MLFMA, where no treatment is done for the low-frequency problem, and with (b) the scaled MLFMA, where the low-frequency problem, is treated exactly the same way as in the IL-MLFMA (i.e., using the method presented in [8]), but the IL concept is not used.

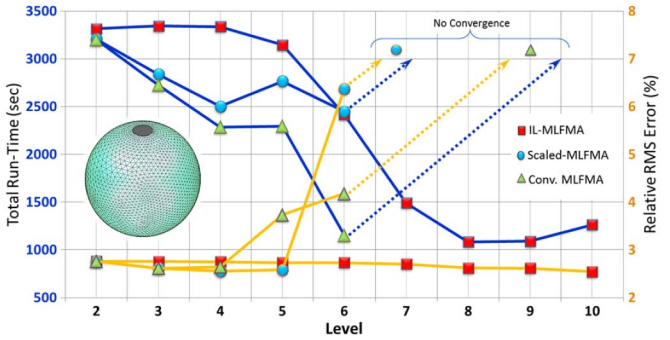


Fig. 10. Total run times and relative RMS errors versus the number of levels for three versions of the MLFMA. The geometry in Fig. 9 is used at $f = 3.0$ GHz. The square, circle, and triangle markers are used to separate three MLFMA versions. The black (blue) lines and gray (orange) lines along with corresponding vertical axis on the left and right show the total run times and the relative RMS errors, respectively.

Fig. 10 (left and right) illustrates the total run time [black (blue) lines are used] and the relative RMS error [gray (orange) lines are used] versus the number of levels for the three versions of MLFMA, respectively. Considering the accuracy, all three versions are comparable with each other up to level 4. However, due to a high multiscale factor, the results obtained from the conventional and scaled MLFMAs start to become inaccurate after level 4 and both versions fail to converge for a large number of levels (no data are available for levels higher than 6 for both versions, which is shown by the dashed lines in Fig. 10). On the other hand, the efficiency of the IL-MLFMA is much better than those of the both versions for the optimal MBPs that correspond to the eighth and ninth levels for IL-MLFMA, where the accuracy remains almost stable. This is more evident regarding larger problems involving larger numbers of unknowns, where more levels are required. Therefore, to demonstrate the superiority of the IL-MLFMA, we investigate three larger problems. Table II summarizes the solutions of scattering problems involving four discretizations of the PEC sphere shown in Fig. 9 ($R = 5$ cm at 300 MHz) formulated with the MFIE. The first model is the same as before, involving 11 343 RWG functions with a multiscale factor of 110. The other models are obtained by mesh refinement, leading to 45 372, 181 488, and 725 952 RWG functions, respectively, retaining the same multiscale factor. Note that the conventional MLFMA results are not included either due to very large errors or due to convergence problems. According to these results: 1) the IL-MLFMA is two to six times more efficient than the scaled MLFMA and 2) the accuracy is also more than six times better than the scaled version, for a large problem.

To find out the performance of the IL-MLFMA in near-zone fields, we use the third sphere example given in Table II consisting of 181 488 RWG functions. Fig. 11(a) and (b) illustrate the magnitudes of the total electric field on the $xy$ plane, inside the PEC sphere as well as in the vicinity of it, assuming that the center of the sphere is at the origin. The sphere is illuminated by a unit plane wave at 300 MHz,

TABLE II

PERFORMANCE COMPARISON BETWEEN THE IL-MLFMA AND THE SCALED-MLFMA APPLIED TO FOUR DENSELY MESHED SPHERES OF $R = 5$ cm AT $f = 300$ MHz WITH A MULTISCALE FACTOR OF 110

| Number of Unknowns | 11,343 | | 45,372 | | 181,488 | | 725,952 | |
|---|---|---|---|---|---|---|---|---|
| Method | IL | Scaled [1] | IL | Scaled[2] | IL | Scaled[3] | IL | Scaled [4] |
| MBP | 100 | - | 100 | - | 100 | - | 100 | - |
| Level | 8 | 3 | 9 | 6 | 10 | 8 | 11 | - |
| Total Time (sec) | 1331 | 2674 | 7018 | 22131 | 27171 | 184550 | 136441 | - |
| Near-Field Time (sec) | 399 | 2315 | 1898 | 16679 | 4030 | 26128 | 15568 | - |
| Solution Time (sec) | 917 | 346 | 5023 | 5394 | 22624 | 158039 | 113578 | - |
| Iteration | 61 | 60 | 64 | 64 | 66 | 196 | 67 | - |
| Rel. RMS Error (%) | 2.45 | 2.60 | 1.49 | 1.69 | 1.37 | 9.04 | 1.37 | - |

[1] The best solution regarding efficiency and accuracy [2] The best result among two available solutions

[3] The only available solution [4] No solution due to convergence problem

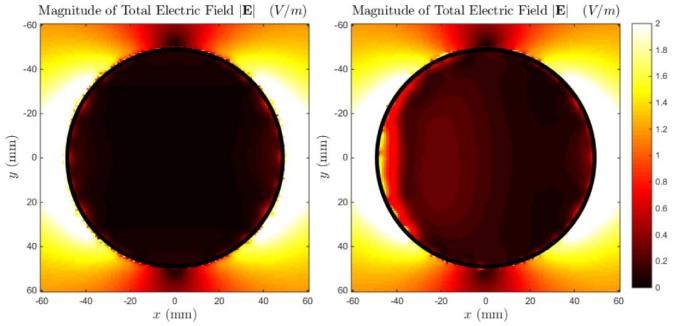


(a) (b)

Fig. 11. Near-field total electric field values on the $xy$ plane for a PEC sphere of radius $R = 50$ mm illuminated by a unit plane wave at 300 MHz, propagating in the $z$ direction with the electric field polarized in the $x$ direction. The sphere is chosen to be the third example given in Table II with 181 488 RWG functions. (a) Solution using the IL-MLFMA with 7.71% RMS error, by expecting zero fields inside the sphere. (b) Solution using the scaled MLFMA with 19.06% RMS error, by expecting zero fields inside the sphere.

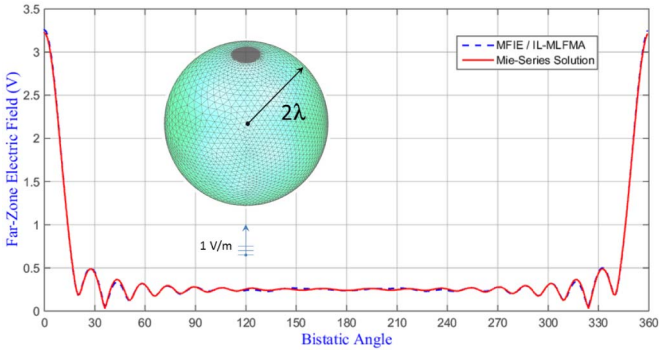


Fig. 12. Solution of a scattering problem using the IL-MLFMA, involving a large PEC sphere of radius $R = 0.5$ m ($2\lambda$) illuminated by a unit plane wave at $f = 1.2$ GHz. The discretized surface consists of 722 529 basis functions possessing a multiscale factor of 375.

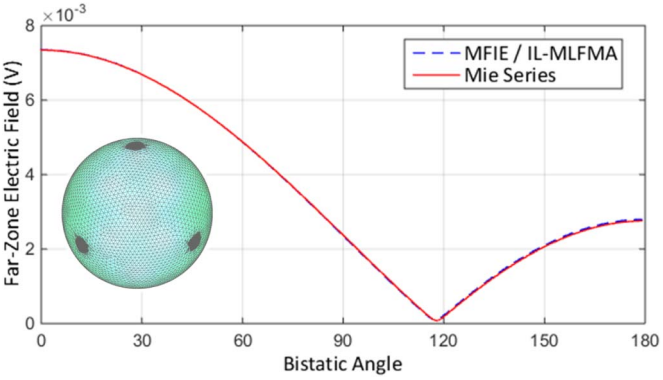


Fig. 13. Far-zone electric field scattered from a PEC sphere of radius $R = 5$ cm with a more complicated discretization as shown in the inset, illuminated by a unit plane wave at 300 MHz. The sphere contains six dense mesh regions aligned with the positive and negative directions of $x$, $y$, and $z$ axes, where only three of them are visible in the figure. The multiscale factor is about 100, leading to 557 184 RWG functions.

propagating in the $z$ direction with the electric field polarized in the $x$ direction. Fig. 11(a) shows the IL-MLFMA solution (possessing a far-field relative RMS error of 1.37%), while Fig. 11(b) shows the only available scaled-MLFMA solution (possessing a far-field relative RMS error of 9.04%). High level of error can be distinguished in the latter especially inside the sphere, where a zero electric field is expected. The RMS error values for these solutions are 7.71% and 19.06%, respectively.

To demonstrate how the IL-MLFMA performs for electrically larger problems, we use a sphere similar to the one shown in Fig. 9 with $D = 2R = 1$ m ($4\lambda$) at $f = 1.2$ GHz. The sphere is discretized with 722 529 unknowns, leading to a multiscale factor of 375. The solution is based on 12 levels of the IL-MLFMA with a population threshold of 100. The Mie-series solution is also depicted in Fig. 12 for comparison. Both solutions match very well with each other despite of a small discrepancy originating from the approximate method used for low-frequency treatments.

Finally, we consider a PEC sphere with a more complicated discretization including multiple overmeshed areas, as illustrated in the inset of Fig. 13. In Fig. 13, three among six highly overmeshed areas, which are aligned with the positive and negative directions of the $x$-, $y$-, and $z$-axis over the sphere, can be seen. A refined version of this mesh with a multiscale factor of 100 is used at $f = 300$ MHz, containing 557 184 RWG functions. Fig. 13 depicts the far-zone electric

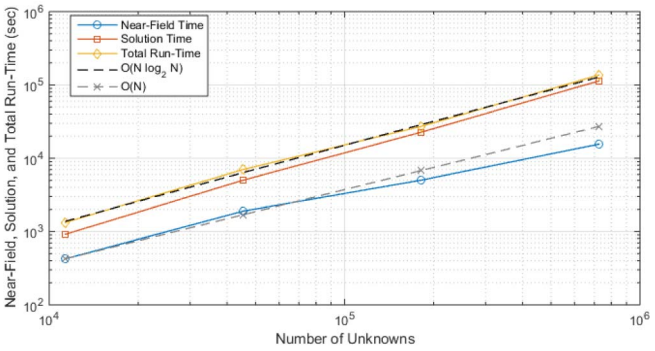


Fig. 14. Three important processing times, i.e., the near-field time, the solution time, and the total run time for four scattering problems given in Table II.

field as a function of the bistatic angle, along with the Mie-series solution, where 0° and 180° correspond to the forward-scattering and backscattering directions, respectively. It is seen that there is a very good agreement between the Mie-series results and the values obtained with the IL-MLFMA. A small amount of discrepancy is originated from the approximate method in the low-frequency regime and it is not related to the proposed IL structure. Note that, for the same reason, the relative RMS error of 1.37% given in Table II does not change for very fine meshes, i.e., when the discretization error is minimized and the low-frequency inaccuracies dominate the total error.

The proposed broadband solver shows $\mathcal{O}(N \log^{\alpha} N)$ computational complexity, where $\alpha$ $(1 \leq \alpha \leq 2)$ depends on how deep we are getting into low-frequency regime after recursively clustering the object based on the given population threshold. The number of levels follows an $\mathcal{O}(\log N)$ complexity, where the base of the logarithm mainly depends on the population statistics. By reusing the information given in Table II, all three important processing times, i.e., the near-field time, the solution time, and the total run time of the proposed method, are plotted in Fig. 14. For comparison purposes, both $\mathcal{O}(N \log_2 N)$ and $\mathcal{O}(N)$ lines are also plotted (in dashed black and gray lines, respectively), where the former passes through the first point of the total run time line and the latter passes through the first point of the near-field line. As it can be seen from Fig. 14, the efficiency of the proposed method manifests itself for larger and more complicated geometries with a higher number of unknowns. This is more evident comparing the number of near-field interactions (the blue line) and the $\mathcal{O}(N)$ line. Even though the solution and near-field computation times show a bit higher and lower complexities with respect to their dedicated reference dashed lines, the total run time closely follows the claimed linearithmic complexity.

## V. Conclusion

An efficient and versatile broadband MLFMA, referred to as the IL MLFMA, is presented to solve multiscale electromagnetic problems for PEC objects. The concept of IL tree structures is introduced, where only the OCBs are divided into smaller ones for a given population threshold, leading to a nonuniform clustering. Thus, protrusions of RWG functions from the boxes are minimized, which improves the accuracy, and the total number of interacting boxes is reduced, which improves the efficiency. The error of the proposed structure is almost independent of the levels. Consequently, for the geometries that can be discretized with nonuniform meshes with a large multiscale factor, the IL-MLFMA is always more efficient than the conventional one for the same accuracy, and it is more accurate if the efficiency is comparable, as demonstrated with some canonical examples. Furthermore, the IL-MLFMA recovers the conventional MLFMA for uniform meshes, if desired. As a result, all other computational methods that can be combined with the conventional MLFMA can also be used in conjunction with the proposed IL-MLFMA.

## References

[1] R. F. Harrington, *Field Computation by Moment Methods*. New York, NY, USA: Macmillan, 1968.
[2] R. Coifman, V. Rokhlin, and S. Wandzura, "The fast multipole method for the wave equation: A pedestrian prescription," *IEEE Antennas Propag. Mag.*, vol. 35, no. 3, pp. 7–12, Jun. 1993.
[3] J. Song, C.-C. Lu, and W. C. Chew, "Multilevel fast multipole algorithm for electromagnetic scattering by large complex objects," *IEEE Trans. Antennas Propag.*, vol. 45, no. 10, pp. 1488–1493, Oct. 1997.
[4] E. Bleszynski, M. Bleszynski, and T. Jaroszewicz, "AIM: Adaptive integral method for solving large-scale electromagnetic scattering and radiation problems," *Radio Sci.*, vol. 31, no. 5, pp. 1225–1251, Sep./Oct. 1996.
[5] S. M. Seo and J.-F. Lee, "A single-level low rank IE-QR algorithm for PEC scattering problems using EFIE formulation," *IEEE Trans. Antennas Propag.*, vol. 52, no. 8, pp. 2141–2146, Aug. 2004.
[6] S. Kurz, O. Rain, and S. Rjasanow, "The adaptive cross-approximation technique for the 3D boundary-element method," *IEEE Trans. Magn.*, vol. 38, no. 2, pp. 421–424, Mar. 2002.
[7] W. C. Chew, E. Michielssen, J. M. Song, and J. M. Jin, *Fast and Efficient Algorithms in Computational Electromagnetics*. Boston, MA, USA: Artech House, 2001.
[8] Ö. Ergül and B. Karaosmanoğlu, "Approximate stable diagonalization of the Green's function for low frequencies," *IEEE Antennas Wireless Propag. Lett.*, vol. 13, pp. 1054–1056, 2014.
[9] L. Greengard, J. Huang, V. Rokhlin, and S. Wandzura, "Accelerating fast multipole methods for the Helmholtz equation at low frequencies," *IEEE Comput. Sci. Eng.*, vol. 5, no. 3, pp. 32–38, Jul. 1998.
[10] H. Cheng *et al.*, "A wideband fast multipole method for the Helmholtz equation in three dimensions," *J. Comput. Phys.*, vol. 216, no. 1, pp. 300–325, Jul. 2006.
[11] X.-M. Pan, J.-G. Wei, Z. Peng, and X.-Q. Sheng, "A fast algorithm for multiscale electromagnetic problems using interpolative decomposition and multilevel fast multipole algorithm," *Radio Sci.*, vol. 47, no. 1, pp. 1–11, Feb. 2012.
[12] J. G. Wei, Z. Peng, and J. F. Lee, "Multi-scale electromagnetic computations using a hierarchical multi-level fast multipole algorithm," *Radio Sci.*, vol. 49, no. 11, pp. 1022–1040, Nov. 2014.
[13] I. Bogaert, J. Peeters, and F. Olyslager, "A nondirective plane wave MLFMA stable at low frequencies," *IEEE Trans. Antennas Propag.*, vol. 56, no. 12, pp. 3752–3767, Dec. 2008.
[14] I. Bogaert and F. Olyslager, "A low frequency stable plane wave addition theorem," *J. Comput. Phys.*, vol. 228, no. 4, pp. 1000–1016, Mar. 2009.
[15] H. Shao, J. Hu, Z. Nie, and L. Jiang, "Simulation of multiscale structures using equivalence principle algorithm with grid-robust higher order vector basis," *J. Electromagn. Waves Appl.*, vol. 28, no. 11, pp. 1333–1346, 2014.
[16] J.-G. Wei, Z. Peng, and J.-F. Lee, "Multiscale electromagnetic computations using a hierarchical multilevel fast multipole algorithm," *Radio Sci.*, vol. 49, no. 11, pp. 1022–1040, Nov. 2014.
[17] F. Vipiana, P. Pirinoli, and G. Vecchi, "A multiresolution method of moments for triangular meshes," *IEEE Trans. Antennas Propag.*, vol. 53, no. 7, pp. 2247–2258, Jul. 2005.
[18] M. Vikram, H. Huang, B. Shanker, and T. Van, "A novel wideband FMM for fast integral equation solution of multiscale problems in electromagnetics," *IEEE Trans. Antennas Propag.*, vol. 57, no. 7, pp. 2094–2104, Jul. 2009.

[19] I. Lashuk *et al.*, "A massively parallel adaptive fast multipole method on heterogeneous architectures," *Commun. ACM*, vol. 55, no. 5, pp. 101–109, May 2012.
[20] T. J. Giese and D. M. York, "Extension of adaptive tree code and fast multipole methods to high angular momentum particle charge densities," *J. Comput. Chem.*, vol. 29, no. 12, pp. 1895–1904, Sep. 2008.
[21] K. Y. Sanbonmatsu and C.-S. Tung, "High performance computing in biology: Multimillion atom simulations of nanoscale systems," *J. Struct. Biol.*, vol. 157, no. 3, pp. 470–480, Mar. 2007.
[22] L. Ying, G. Biros, D. Zorin, and H. Langston, "A new parallel kernel-independent fast multipole method," in *Proc. ACM/IEEE Conf. Supercomput.*, Nov. 2003, p. 14.
[23] W.-B. Kong, H.-X. Zhou, W.-D. Li, G. Hua, and W. Hong, "The MLFMA equipped with a hybrid tree structure for the multiscale EM scattering," *Int. J. Antennas Propag.*, vol. 2014, Jan. 2014, Art. no. 281303.
[24] S. M. Rao, D. R. Wilton, and A. W. Glisson, "Electromagnetic scattering by surfaces of arbitrary shape," *IEEE Trans. Antennas Propag.*, vol. 30, no. 3, pp. 409–418, May 1982.

**Manouchehr Takrimi** (S'13) was born in Urmia, Iran, in 1971. He received the B.Sc. degree in telecommunication engineering from Tehran University, Tehran, Iran, in 1993, and the M.S. degree in telecommunication engineering from the Isfahan University of Technology, Isfahan, Iran, in 1995. He is currently pursuing the Ph.D. degree with the Electrical and Electronics Engineering Department, Bilkent University, Ankara, Turkey.

His current research interests include the computational electromagnetics and fast solvers.

**Özgür Ergül** (S'98–M'01–SM'13) received the B.Sc., M.S., and Ph.D. degrees from Bilkent University, Ankara, Turkey, in 2001, 2003, and 2009, respectively, all in electrical and electronics engineering.

He served as a Teaching and a Research Assistant with the Department of Electrical and Electronics Engineering, Bilkent University, from 2001 to 2009. He was with the Computational Electromagnetics Group, Bilkent University, from 2000 to 2005, and with the Computational Electromagnetics Research Center, Bilkent University, from 2005 to 2009. In 2009, he joined the Department of Mathematics and Statistic, University of Strathclyde, Glasgow, U.K., as a Lecturer. He was also a Lecturer with the Centre for Numerical Algorithms and Intelligent Software, U.K. In 2012, he joined the Department of Electrical and Electronics Engineering, METU, where he is currently an Assistant Professor. He is the Principal Investigator of the CEMMETU Research Group, Ankara. He is the author of the undergraduate textbook entitled *Guide to Programming and Algorithms Using R* (Springer), and the co-author of the graduate textbook entitled *The Multilevel Fast Multipole Algorithm (MLFMA) for Solving Large-Scale Computational Electromagnetics Problems* (Wiley-IEEE) and over 170 journal and conference papers. His current research interests include fast and accurate algorithms for the solution of electromagnetics problems involving large and complicated structures, integral equations, iterative methods, parallel programming, and high-performance computing.

Dr. Ergül was a recipient of the 2007 IEEE Antennas and Propagation Society Graduate Fellowship, the 2007 Leopold B. Felsen Award for Excellence in Electrodynamics, the 2010 Serhat Ozyar Young Scientist of the Year Award, the 2011 URSI Young Scientists Award, the 2013 Science Academy Young Scientists Award, the first ever (2013) ACES Early Career Award, the 2013 Parlar Foundation Research Incentive Award, the 2014 Parlar Foundation Instructor of the Year Award, and the 2014 TUBITAK Incentive Award. He is also serving as an Associate Editor of the *IEEE Antennas and Propagation Magazine* (Open Problems in CEM Column) and an Editorial Board Member of *Scientific Reports* (Nature Publishing Group).

**Vakur B. Ertürk** (M'00) received the B.Sc. degree in electrical engineering from Middle East Technical University, Ankara, Turkey, in 1993, and the M.S. and Ph.D. degrees from The Ohio State University, Columbus, OH, USA, in 1996 and 2000, respectively.

He is currently with the Electrical and Electronics Engineering Department, Bilkent University, Ankara. His current research interests include the analysis and design of planar and conformal arrays, computational electromagnetics, sensors for structural health monitoring, magnetic resonance imaging, scattering from and propagation over large terrain profiles, and high-frequency techniques.

Dr. Ertürk was a recipient of 2005 URSI Young Scientist and 2007 Turkish Academy of Sciences Distinguished Young Scientist Awards. He served as the Secretary/Treasurer of the IEEE Turkey Section and the Turkey Chapter of the IEEE Antennas and Propagation, Microwave Theory and Techniques, Electron Devices and Electromagnetic Compatibility Societies.